Biotechnol Lett (2020) 42:151–170
https://doi.org/10.1007/s10529-019-02764-5

ORIGINAL RESEARCH PAPER

Myco-engineered gold nanoparticles from *Jahnula aquatica* coated with ampicillin/amoxicillin and their antibacterial and anticancer activity against cancer cells

Mohamed A. Mohamed

Received: 23 July 2019 / Accepted: 11 November 2019 / Published online: 15 November 2019

Abstract
Introduction Antibiotics play an important role in medical treatments. However, the multidrug resistance (MDR) bacteria impairs their functionality. Therefore, drug delivery represents the solution for this problem. Many techniques and methods are used in drug delivery, however nanoparticles conjugated drug is one of the most effective and promising techniques. The current work investigates a one-step method of extracellular biosynthesis of gold nanoparticles (AuNPs) and their biocompatibility in antibiotic delivery, where the synthesized AuNPs were loaded with Ampicillin/Amoxicillin.
Results Both ampicillin and amoxicillin antibiotics are successfully conjugated with the Au NPs surface (the potential efficiency), especially, at the smaller particle size. Where, the Au NPs with particle size of 8 m size reveals a promising activity against cancer cells with 48 μg/mL inhibitory concentration (IC_{50}) after 24 h of their exposure to HeLa cells, and induction of apoptosis was also noticed on HeLa treated cells.
Conclusions The bio-synthesised Au NPs using *Jahnula. aquatica* fungi show a promising nanocarrier biocompatibility drug delivery system in cancer clinical treatments, in particular for antibiotics delivery antibiotics in pharmaceutical applications with large-scale commercial production. To the best of our knowledge, freshwater fungi have never been exploited for AuNPs synthesis.

Keywords Gold nanoparticles · Antibiotics · Antibacterial and anticancer · Drug delivery

M. A. Mohamed (✉)
Nanotechnology & Advanced Nano-Materials Laboratory (NANML), Plant Pathology Research Institute, Agricultural Research Center, Giza 12619, Egypt
e-mail: mohammed_sharouny@yahoo.com

M. A. Mohamed
Instituto de Biología Molecular y Celular de Plantas (Consejo Superior de Investigaciones Científicas-Universidad Politécnica de Valencia), Avenida de los Naranjos, 46022 Valencia, Spain

Introduction

Antibiotics play an important role in curing almost of infection problems (Delcaru et al. 2017). However, the excessive usage have impaired their function that appears as a resistance by bacteria against the curing drug or what is know as multi-drug resistance (MDR), which is real global threat and one of the greatest challenges for healthcare practitioners (Lien et al. 2017). The β-lactam antibiotics represent a wide potential base against different resistant drug bacteria (Sotgiu et al. 2016), however, the level of antibiotic bacterial resistance is increasing contentiously, decreasing the antibiotic efficiency (Baroud et al. 2013). According to the global antibiotic free curing plan, new alternative strategies have been proposed

overcome the continued outgrowth of antibiotic bacterial resistance (Tang et al. 2016). Antibiotics synergism with the same/different mechanism is widely common and leads to a clinical delay of antibiotic resistance if utilized wisely (Miliani et al. 2011; Sun et al. 2014; Yang et al. 2016; Paczkowska et al. 2016). Another promising solution is to insert an antibiotic molecules inside a complex agent from in vivo hydrolysis in the human body. However, more efforts are required to confirm the degree of safety and stability of these complexes. Recently, different nanocarriers are available for constructing unique types of drug delivery systems at the nanoscale including liposomes, dendrimers, polymers, carbon materials, silicon, and magnetic nanoparticles (NPs) (Brown et al. 2012; Rastogi et al. 2012; Thomas et al. 2014; Gannimani et al. 2016; Kandimalla et al. 2016; Roy et al. 2018). Consequently, extensive researches are still ongoing in the delivery system area to address the most reliable and effective methods to fix the above mentioned problem.

Nanoparticles conjugated drug is one of the most effective and promising techniques in intracellular delivering antibiotics. Among all nanomaterials, gold nanoparticles (Au NPs) have attracted the intension due to their cytotoxic effect on cancer cells without a damage of the normal cells, which introduce these NPs in cancer clinical treatment (Cui et al. 2012; Patil et al. 2017). Their wide usage refers to the high safety profile, biocompatibility with the human body, unique covalent binding and electrostatic adsorption of their surface (Kandimalla et al. 2016; Mori and Hegmann 2016; Foo et al. 2017; Kim et al. 2017; Maity et al. 2018). Au NPs are synthesized using in several physical and chemical methods, and almost of these methods are energy intensive (Dhamecha et al. 2016; Yuan et al. 2017a, b). However, many synthesis methods involves toxic chemicals that precluding their use in numerous pharmaceutical and medical areas (Yuan et al. 2017a, b). Recently, biological synthesis of gold nanoparticles has become more attractive than physical and chemical methods due to safety, low cost and various shape (size, and morphology) (Kasthuri et al. 2009; Balasooriya et al. 2017). Fungi are good option in comparison with other biological methods such as bacteria and plants. This is because of fungi contains high amount of proteins, enzymes, and other biomolecules that have the ability of redox capacity, increasing the productivity during the nanomaterials synthesis (Kasthuri et al. 2009). Till now, there are more than six hundred fungal species of ascomycetes and anamorphic that have been discovered from freshwater ecosystems. However, few studies that have focused on the chemical/biological properties (Hernández-Carlos and Gamboa-Angulo 2011). Therefore, not much information are available about their metabolites potential and its properties that may be wisely used and exploited in different applications including nanotechnology.

In this work we investigate the extracellular synthesis and drug delivery functionality of mycogenic gold nanoparticles using the *Jahnula aquatica* fungus. This is achieved via uploading Ampicillin/Amoxicillin antibiotics on top of different sizes of gold NPs. This is in addition to the evaluation of the anticancer effect against human cancer cell lines with fundamental molecular techniques to understand the cytotoxicity mechanism against HeLa cancer cells in vitro. As far of author's knowledge, there is no reported results in the exploitation of the freshwater fungi generally in nanomaterials synthesis.

Materials and methods

Chemicals

Gold chloride hydrate (analytical grade) was purchased from Sigma-Aldrich. The Au NPs were loaded with Ampicillin (Amp.) and Amoxicillin (Amox) purchased from Astra-Zeneca (Boston, Massachusetts, USA) in a Pharmaceutical analytical grade. Human cervical carcinoma cell lines (HeLa) were obtained from the American Type Culture Collection (ATCC, MD, USA).

The freshwater fungus

The freshwater fungus *Jahnula aquatica* was isolated according to the single-spore isolation technique (Choi 1999) from submerged woody debris collected from Jućar River in Spain 2015, and morphologically identified following the corresponding keys and the relevant literatures (Goh and Hyde 1999). However, species identification under genus Jahnula, based only on morphological criteria, may not prove absolutely accurate. Thus, molecular identification was applied for additional confirmation. Thus, the genomic DNA of the fungal isolate was purified as reported by (Abdel-Hafez

et al. 2016). The ITS was amplified and sequenced. Alignment with *Jahnula aquatica* rDNA in NCBI GenBank (JN942348.1) resulted in a 100% identity match.

Biosynthesis of gold nanoparticles (AuNPs)

Au NPs were biologically synthesized using the freshwater fungus *Jahnula aquatica* aqueous extract as reducing/capping agent. The synthesis process was conducted with varied reaction conditions to obtain different Au NPs sizes of 8 nm, 20 nm and 60 nm, the details are reported elsewhere with some modification (Poojary et al. 2016).

Au NPs- antibiotics conjugation

The conjugation of Au NPs and antibiotics were prepared by adding 4 ml of the antibiotics under study in (1 mg/ml in PBS, pH 7.4) concentration drop wised to 10 ml from the Au NPs in different sizes of 8 nm, 20 nm and 60 nm with continuing magnetic stirring for two hours at room temperature. The change in the surface plasmon resonance (SPR) of the conjugated Au NPs was measured using Uv–visible spectroscopic analyse in the range of 200–800 nm. The extra unloaded antibiotic molecules were collected by centrifugation the Au NPs mixture solution at 20,000 rpm for 20 min. The percentage (%) of loading efficiency in percentage of antibiotic content attached on the Au NPs surface were evaluated by measuring the unloaded antibiotics content in the residual supernatant of the mixture solution by UV measurements in the range of 300 and 295 nm for Ampicillin and Amoxicillin, using Eqs. 1 and 2, respectively (Rohman et al. 2015).

$$\text{Drug loading efficiency } (\%) = [(\text{Total antibiotic} - \text{antibiotic in supernatant})/\text{total amount of the antibiotics}] \times 100 \quad (1)$$

$$\text{Drug content } (\%) = [(\text{Total antibiotic} - \text{antibiotic in supernatant})/\text{amount of AuNPs} + (\text{Total antibiotic} - \text{antibiotic in supernatant})] \times 100 \quad (2)$$

Moreover, we measured the possibility of adsorbed antibiotics in the inner surface of the centrifugation tube by centrifuging 3 ml mixture solution from both Ampicillin and Amoxicillin (1 mg/ml) at 30,000 rpm for 20 min. The results show the same antibiotic content the produced supernatant, which excludes the possibility of Amp./Amox. adsorption in the centrifuge wall. And the results of Uv spectroscopic analysis of supernatant excludes the interfering possibility of the Au NPs supernatant with Ampicillin/Amoxicillin as well. The scanning spectra indicated the lacking of any interfering absorption at the measurement range of wavelengths. The abbreviations AuNPs, Amp-AuNPs and Amox-AuNPs were used to refer the formed gold nanoparticles, Ampicillin conjugated AuNPs and Amoxicillin conjugated gold nanoparticles, respectively, while the subscripted number adjacent to the proposed abbreviation refers to nanometer size of the formed gold nanoparticles.

Au NPs characterization

UV–visible spectrometric analysis

The gold solution was sampled for different times to monitor the bio-reduction of Au NPs and also to evaluate their stability over 1 month. The UV–visible spectrum of the sampled solution was measured using a UV–visible spectrophotometer (Shimadzu UV-1800) at wavelengths ranged in the 200–800 nm.

High resolution transmission electron microscopy (HR-TEM)

The Au NPs shape and size characteristics were measured using a JEOL 3010 instrument operated at an accelerating voltage of 300 kV. Briefly, the HR-TEM samples were prepared by drop coating Au NPs solution onto carbon coated copper TEM grids. The prepared films on the TEM grids were allowed to stand for 5 min for dryness, while the extra solution was erased using a blotting paper.

The dynamic light scattering (DLS) and zeta potential analysis

The NPs size and Zeta value of Au NPs in aqueous phase potential were evaluated using particle size analyser (ELSZ-1000, Otsuka, Japan).

X-ray diffraction (XRD) analysis

The XRD technique was examine crystallinity of Amp/Amox before and after the conjugation with the Au NPs using a Bruker AXS D8 Advance X-ray diffractometer with Cu K radiation of wavelength 1.541 Å and scanning angle 2 in (10°–90°) range.

Fourier transform infrared (FT-IR) analysis

FT-IR analysis was performed to confirm the conjugation of Amp/Amox with theAu NPs. 10 mg of the Amp/Amox conjugated Au NPs powder mixed with a pinch of potassium bromide (Himedia FT-IR graded) in a crucible were used for FT-IR measurement. The mixture was pelletized by hydraulic press and the pellet was analysed in Jasco FT/IR-6300 equipped with JASCO IRT-7000 Intron Infrared Microscope with transmittance at range a 4 cm^{-1} resolution (JASCO, Tokyo, Japan).

Drug release

The degree of antibiotics release was investigated via the membrane dialysis technique in vitro as reported in (Harsha 2012; Onuigbo et al. 2016; Yuan et al. 2017a, b). 5 ml of antibiotic was loaded on AuNPs (3 mg/ml in PBS, pH 7.4) and left over-night soaked dialysis bags, (MWCO 3500 Daltons). The inoculated bags were slowly transferred to a sterilized closed bottles containing 50 ml of the same buffer and maintained at 37 °C with shaking at 100 rpm. A small amount (5 ml) from the released media were taken over a course of time and replaced by fresh phosphate buffer solution (PBS) medium. The amount of Ampicillin and Amoxicillin released in the media was analyzed by UV–visible spectrophotometer (Shimadzu UV-1800) at 318 nm and 295 nm, respectively.

Au NPs antibacterial activity

Bacterial Antibiotic susceptibility

Different infectious bacterial isolates were collected with a permission from the clinical laboratories of Kasr El-Ainy Hospitals, University of Cairo, Egypt. The Gram negative bacteria were purified and maintained following the standard protocols and confirmed to specific species according to Bergey's manual (Boone et al. 2001). The antibiotic susceptibility against each bacterial isolate was evaluated following disk diffusion assay method under the Clinical and Laboratory Standards Institute guidelines (CCLS) in 2015. The bacterial isolates: *Pseudomonas aeruginosa*, *Staphylococcus aureus* (MRSA), and *Enterobacter aerogenes* were selected as a result of their high resistant activity against both antibiotics (Amp and Amox). Identification of MRSA was confirmed according to the recommendations of the National Committee for Clinical Laboratory Standards. Thus, they were selected for the present study.

The minimum inhibitory concentrations (MICs)

The MICs of Amp, Amox and their conjugation with the AuNPs were determined for the used bacteria using the micro titre assay method. Each bacterial strain was firstly inoculated on a fresh Muller-Hinton (MH) growth medium and incubated for 12 h at 37 °C. Then, 2- fold serial dilutions from Amp and their equivalent amounts from Amp-AuNPs and from Amox-AuNPs respectively were prepared in a concentration of (640–1.25 µg/ml) in MH broth medium. The cultivated bacterial plates were diluted to 1 × 106 CFU/ml concentration and then inoculated with the antibiotic dilutions. All the inoculated bacterial plates were placed for incubation at 37 °C for 24 h. All the practical experiments were repeated three times and the free AuNPs were served as a negative control. The MIC values for all treatments were considered as the least concentration of used agent that is completely impair the bacterial colony growth.

Antibiotic's loaded AuNPs time kill test

The rate of antibiotic's loaded AuNPs in killing the resistant bacteria under the study was carried out by

performing a time kill assay experiments for both antibiotics individually (Amp, Amox) and also in loading form (Amp-AuNPs8, Amox-AuNPs8) against *Pseudomonas aeruginosa* and *Staphylococcus aureus* and compare them with untreated ones. Briefly, the bacterial strains were cultured in Luria–bertani (LB) medium reaching 1×10^6 CFU/ml. Then, the bacterial suspension for each strain was challenged with the treatments: Amp, Amp-AuNPs8, Amox and Amox-AuNPs8 till final concentration 2.5 µg/ml for *S. aureus* and 1.25 µg/ml for *P. aeruginosa* and incubated at 37 °C. At different time intervals (0, 1, 2, 4, 8, 12, and 24 h), the samples were withdrawn and diluted 10 folds to count the number of viable bacterial colonies using the surface drop method (Shameli et al. 2012).

Cytotoxicity analysis of AuNPs

The cytotoxicity of the 8 nm Au NPs on the proliferation of HeLa cells was analyzed by the MTT (3-(4, 5-dimethylthiazol-2-yl)-2, 5-di phenyl tetra-zolium bromide) assay. Firstly, the, HeLa cancer cells were cultivated in DMEM supplemented with antibiotic agents (penicillin 120 IU/mL and streptomycin 100 IU/mL) and 10% (v/v), fetal bovine serum (FBS) and non-essential amino acids. Then, the cultivated cells were maintained in a humidified atmosphere of 5% Carbon dioxide (CO2) at 37 °C. Briefly, the cells were grown to 1×10^5 cells/well in 96 well plates and then incubated with various different AuNPs concentrations (15, 30, 60, 125, 250 and 500 µg/mL) at 37 °C with 5% CO_2 for 24 h. After treatment with varied AuNPs concentrations, the treated Hela cells were extensively washed with PBS with changing the medium to remove the dead cells. The cytotoxicity and the inhibitory concentration (IC_{50}) was calculated by incubating the treated HeLa cells with 300 µL (1 mg/mL) of MTT for 3 h in 5% CO_2 incubator. The mitochondrial dehydrogenases reduce the MTT medium with the yellow tetrazole characteristic color into purple formazan in the living cells. Higher number of living cells resulted in increasing optical intensity of the purple color. Micro-plate Reader (Bio Rad, M-680) was used to analyze the measurement of MTT assay by color development using a spectrophotometer at 540 nm after the removal MTT solution and cell lysis in DMSO (600 µL). The cytotoxicity level was evaluated following the equation:

$$\% \text{ Cell viability} = (\text{Optical density (OD) in sample well} / \text{Optical density (OD) in control well}) \times 100$$

Apoptotic Effects

Acridine orange (AO) and ethidium bromide (ETBr) stain

The acridine orange/ethidium bromide staining technique was used firstly to measure the apoptosis effect of AuNPs on Hela cells and also to differentiate between active and non active proliferating cells. Briefly, 10 µl of AO/EtBr were gently added to the treated cells on a clean glass slide. The stained slide was then incubated for 5–7 min at 22 °C. The treated cells showing apoptotic characters with and deformed condensed chromatin with fragmented nuclei were observed by the appearance of their red fluorescence in contrast to the normal cells that appear by their shin green fluorescence. This was counted by using epi-fluorescence microscopy (Eclipse 80i, Nikon, Japan) at ×40 magnification with excitation filter centered at 510–590 nm.

DAPI Staining

The nuclear apoptosis of AuNPs was also tested by preparing two equal concentrations (1×10^5) from untreated and treated HeLa cells. The treated cells were washed several times with the phosphate solution and fixed with 3.7% paraformaldehyde in PBS for 1 h under normal temperature, and finally stained with DAPI solution for 15 min at 37 °C. Finally, the epifluorescence microscopy (Eclipse 80i, Nikon, Japan) at ×40 magnification with excitation filter at 510–590 nm was used to investigate the treated cells.

Ultra-thin sections

Ultra-thin sections from the AuNPs treated cancer cells were prepared in order to study the localization of AuNPs inside those cells. HeLa cells were firstly washed with PBS, detached by trypsinization and

centrifuged at 12,000–14,000 rpm for 10–12 min after 24 h incubation with 4 µg/mL AuNPs, and untreated cells were served as control. The medium without nanoparticles was used as control in the experiment. The treated cells were then fixed with 2.5% glutaraldehyde for 24 h, followed by post-fixation in 1% osmium tetroxide for 2 h and dehydrated with different ethyl alcohol concentrations (10%, 20%, 40%, 60%, 70%, and 80%). The dehydrated cells were then treated with 2% Uranyl-acetate in 95% for 1 h followed by 100% ethanol for the same time. Then, the cells were subjected two times to propylene oxide for 15–20 min each, followed by 1:1 propylene-oxide: araldite resin overnight, and infiltration with fresh araldite resin. Finally, the HeLa cells were embedded for 2 days in araldite resin at 60 °C. The ultra-thin sections were then prepared using an ultra-microtome (Leica EM UC6, Netherlands) instrument. The prepared sections were finally stained with 1% uranyl acetate and 0.2% aqueous lead citrate and mounted on a carbon-coated copper grid (carbon type-B, 300 mesh, Ted Pella, Inc., Redding, CA, USA). The prepared stained sections were finally scanned under a Hitachi H-7500 HR-TEM microscope at 100 kV for ultra-structural observations.

DNA fragmentation analysis

The effect of AuNPs on the DNA of HeLa cancer cells was performed following the method presented in (Barbosa et al. 1995). Briefly, the HeLa cells were firstly plated on DMEM medium contained 10% FBS in 6 well plates with a concentration (1×10^6 cells/mL) per well. The plates were incubated under 5% CO2 at 37 °C for 24 h, followed by removing the DMEM medium and extensively washing the plated cells with the Phosphate buffer. Fresh serum free medium was then added and incubated under carbon dioxide at 37 °C for 1 h. The cells were then treated with the IC50 conc. of the formed AuNPs and incubated again for 24 h. The DNA was then extracted from the treated cells as follows: The cells were properly washed with PBS three times; 0.5 ml of lysis buffer was then added followed by incubation for the mixture solution at 37 °C for 1 h. Small aliquots (4 µL) from proteinase K was added with raising the incubation temperature for 50 °C for 3–4 h. Then, About 0.75 mL of phenol:chloroform:isoamyl alcohol (25:24:1) was added, mixed and centrifuged at 12,000–14,000 rpm for 30 min under cooled conditions. Then two equals volumes from sodium acetate (3 M) and ethanol (iced) solutions were slowly poured and the mixture then was incubated for 1 h on ice to precipitate the nucleic acid (DNA). The DNA was then centrifuged at 14,000 rpm for 10–15 min under cooled conditions 4 °C. The supernatant was discarded and the nuclei acid pellets were properly washed with 1.0 mL of 70% ethanol. The genetic (DNA) pellet was then dried and re-suspended in 50 µl of TE buffer. Finally, 10 µg/mL of the treated DNA samples were separated by electrophoresis using a 1% agarose gel at 75 V for 45 min. The gel was stained with ethidium bromide and then subjected to UV irradiation to photograph the nucleic acid (DNA) bands.

Statistical analysis

All the obtained data were statistically analysed using Origin 8.0 version. Three replicates of each experiment were used and the differences between data values were only significant if the p value was < 0.05.

Results and discussion

Au NPs synthesis

The change in color of the gold salt solution from dark yellow to dark wine red ($\sim$ 5 min) after challenging with *J. aquatica*, fungal extract suggests the formation of spherical shaped AuNPs. The UV–vis absorption spectra indicate the appearance of strong absorption peak centered at 540 nm, revealing the formation of gold nanoparticles (Fig. 1a), and confirms the formation of mono-dispersed Au NPs (Shameli et al. 2012). It is worth to mention that the intensity of the absorbance peak and broadness decrease with time progress as shown in (Fig. 1a), which indicates long time stability of the formed Au NPs (Chen and Li 2007). Consequently, the maximum peak intensity is accomplished after 48 h of reaction, meaning that a complete reduction of the $AuCl_4$—ions. These findings indicate that the freshwater fungal extracted *J. aquatica* is a promising natural reducing agent for synthesizing high concentrations of Au NPs at room temperature (26 °C), without any waste products. On the other hand, the obtained results show the formation

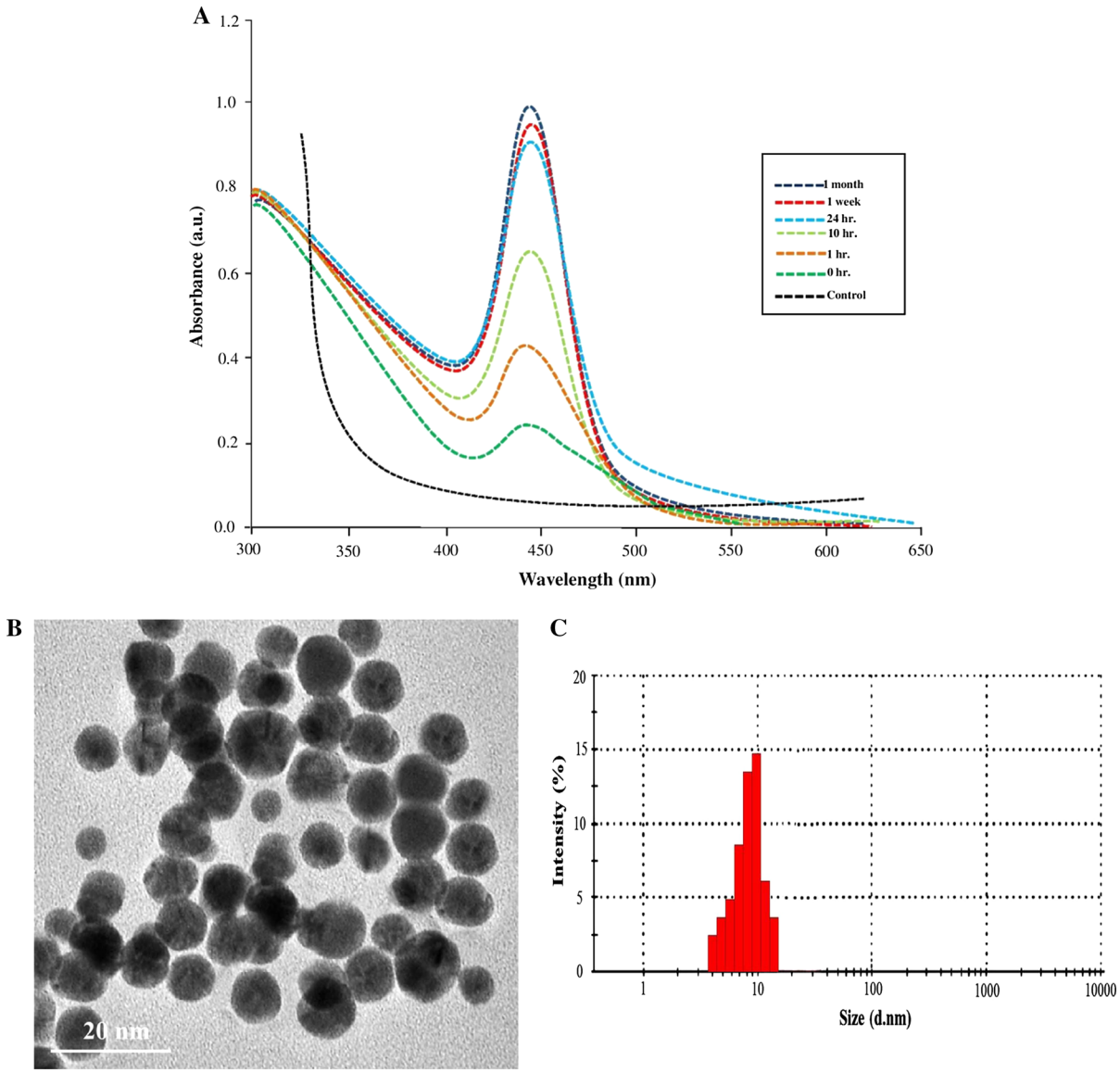

Fig. 1 Mycosynthesis of the formed gold nanoparticles: **a** UV–vis spectra of the formed AuNPs (60 nm) at different times as indicated during the synthesis and after 1 month of storage, **b** HR-TEM image of the mycosynthesized AuNPs at 60 nm scale, and **c** Particle size distribution

of spherical shaped nanoparticles with particle size of 60.4 ± 1.2 nm size and − 43.5 ± 0.5 mV zeta value, indicating an ideal surface charge (Fig. 2a). Furthermore, the zeta potential absolute value indicates a high electrical charge on the Au NPs surface (Fig. 1a), causing a strong repulsive force between the particles to avoid agglomeration and therefore might be liable for their elevated stability and does not change the pink color solution even after 1 month storage at room temperature. Interestingly, the Uv-spectra of the conjugated Au NPs with antibiotics do not show any red/blue shift when in comparison with the spectra of the pure Au NPs. This illustrates the stability of the conjugated AuNPs without aggregation (Fig. 2b).

Characterization of the AuNPs

Raising the reaction temperature to 70 and 90 °C leads to a smaller size of the resultant Au NPs with 20 ± 2.6 and 8 ± 0.9 nm sizes, respectively (Fig. 1b–c, 3a, b).

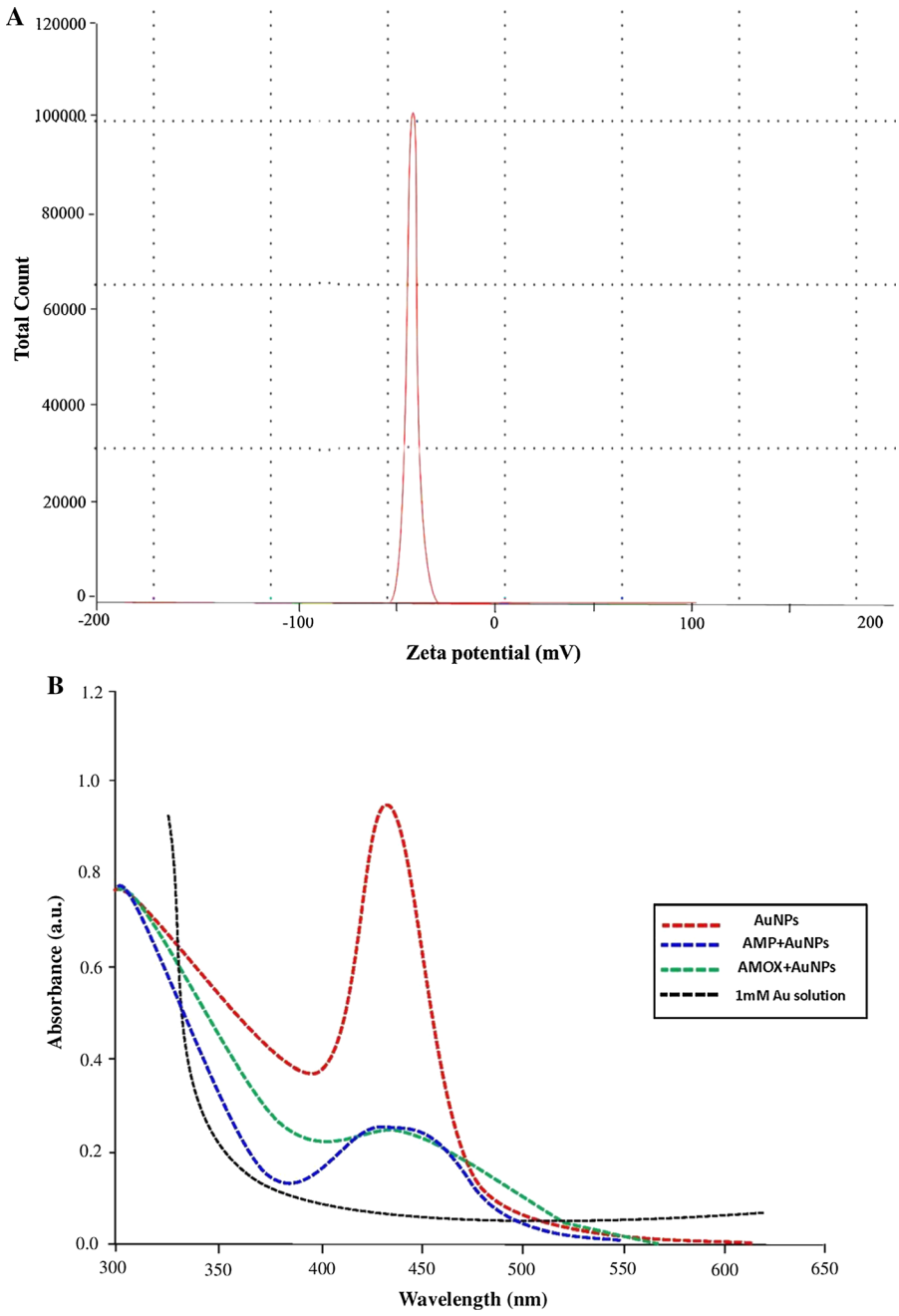

Fig. 2 Characterization of the formed AuNPs: **a** Zeta potential measurements of the formed AuNPs **b** conjugation of gold nanoparticles (8 nm) with Ampicillin (Amp-AuNPs) and Amoxicillin (Amox-AuNPs)

These findings are in agreement with the fact that the reactants consumption is directly proportional with the reaction temperature (Baghizadeh et al. 2015). Data analysis of zeta potential of the free Au NPs indicates the negative surface charge for the particles with 60 nm, 20 nm and 8 nm ($-$ 43.5 $\pm$ 0.5, 42 $\pm$ 1.2, 39.1 $\pm$ 0.2) mV, respectively, revealing the high stability during storage. The slight decrease in zeta value with AuNPs size may be attributed to the increase in the *J. aquatica* concentration that works as a reducing agent during the synthesis process and the process can be accelerated with raising up the reaction temperature. In contrast, the antibiotics conjugated Au NPs show lower zeta potential values, this refers to the positive charges of the loaded antibiotics on the Au NPs surfaces. Thus, uncovers the ramifications of

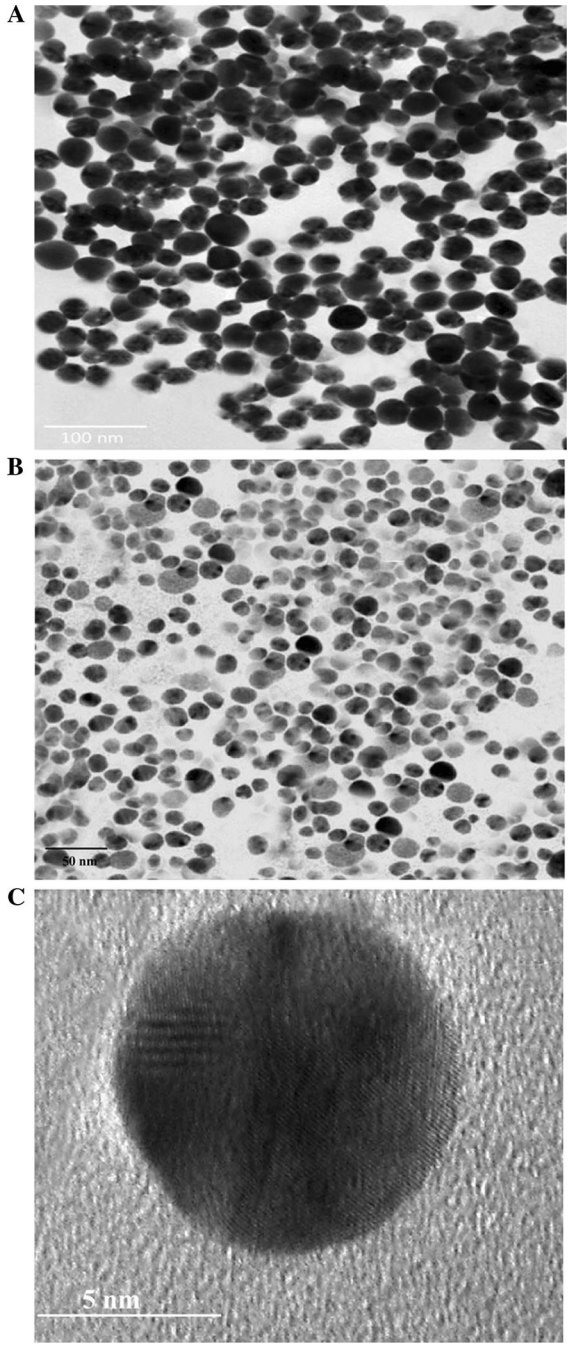

Fig. 3 Optimization and tuning the AuNPs size: **a**, **b** HR-TEM images of the mycosynthesized AuNPs at 20 and 8 nm sizes respectively. **c** Ampicillin loaded gold nanoparticles (8 nm)

intermolecular electrostatic attraction in the Ampicillin/Amoxicillin molecules and the nano gold particles conjugation (Fig. 3c) (Dhar et al. 2008). The XRD patterns for the Ampicillin/Amoxicillin molecules and their conjugation with the Au NPs with particle size of 8 nm are shown in (Fig. 4a). The figure shows multiple peaks, revealing the stability and polycrystalline nature of both antibiotic molecules. These peaks are in correspondence with (111), (200), (220), and (311) crystalline planes of the face-centered cubic structure of the metallic gold (space group Fm3 m, JCPDS File NO. 89-3697), respectively. This is in agreement with the reported results of (Kandimalla et al. 2016). Figure 4b, c shows the FTIR for the Amp, Amox, free Au NPs, AuNPs- Amp-and Amox-AuNPs. The spectra for both Amp and Amp-conjugated Au NPs show broad absorption bands at 3350 cm^{-1} and 3270 cm^{-1} that refers to the stretching vibrations of the (–OH) group in Amp. The observed broadness in these bands may be attributed to the intermolecular existence of the hydrogen bonds in these molecules. The absorption peaks at 2956 cm^{-1} and 2870 cm^{-1} refers to the stretching of N–H and C–H bonds in Amp, respectively. Similarly, the IR spectra for pure Amox and Amox-AuNPs show bands at 3490 cm^{-1} and 3390 cm^{-1} that may be attributed to the stretching vibrations of the (–OH) functional group in Amox. Also, the peaks at 3035 cm^{-1}, and 2870 cm^{-1} may be attributed to the stretching of the amide N–H and the aliphatic C–H bonds, respectively, in contrast with the absorption peak at 3576 cm^{-1}, which coming up due to the stretching of amide (N–H) bond of the pyrroline ring and peaks at 2989 cm^{-1} and 2935 cm^{-1} are for the stretching of the aliphatic C-H in the dimethyl carbanoyl moiety of Amox. Also, the spectra of the Amp and its conjugation with AuNPs also demonstrate the peaks centered at 1779 cm^{-1}, 1740 cm^{-1}, 1657 cm^{-1} and 1585 cm^{-1} refers to stretching vibration of the carbonyl functional group (C=O) found in the β-lactam ring, C=O of the (COO–) functional group, amide I and II bands, of Amp respectively. Furthermore, the peaks at 1464/1447 cm^{-1}, 1390/1235 cm^{-1}, 1075/1035 cm^{-1}, 995/957 cm^{-1}, 897/802 cm^{-1} refer to the stretching of C=N, C=C, N–C–S moiety containing plane vibration, C=C bending and C–C of the Amp, respectively. Similarly, the peaks at 724 cm^{-1} and 692 cm^{-1} refer to the bending of C–N–H and C–O–H bonds of the Amp, respectively. Likewise, the spectra of the Amox and its conjugation with Au NPs (Amox-Au NPs) illustrate that the peaks at 1759 cm^{-1}, 1705 cm^{-1}, 1657 cm^{-1} and 1509 cm^{-1}, which are due to the stretching of carbonyl (C=O) in the (COO–) group, in beta lactam

ring vibration, in amide group, and in amide group (N–H) bending of the Amox respectively. Furthermore, the dual peaks at 1609/1545 cm^{-1}, 1456/1390 cm^{-1}, 989/946 cm^{-1}, 888/817 cm^{-1}, 779/715 cm^{-1} and 554/527 cm^{-1} are attributed to C=C stretching, the aliphatic C–H, CH_3, C–C stretching, C–N–H bending and C–C–C bending, of the Amox respectively. Similarly, the peaks centered at 1335 cm^{-1}, 844 cm^{-1} and 617 cm^{-1} are suggested to be attributed to the aliphatic C–H stretching in pyrroline, C–H and C–O–H bending, of the Amox respectively. Meantime, the symmetric/asymmetric stretching of C–S absorption peaks for both the Amp and the Amox appear at 662 cm^{-1} and 567 cm^{-1} wave length. Most importantly, the IR spectra also shows that a noticeable decrease was recorded in the first peak intensity occurred after the surface conjugation with AuNPs (Amp-AuNPs and Amox-AuNPs) and shifted to a lower wave number by 36–40 cm^{-1}. This significantly reveals that the thio-ether functional group chemisorbed on the AuNPs surface by bonding the sulphur atom (S) with the metallic gold surface. Assignment of the above produced peaks either in the free formed gold nanoparticles or those conjugated with Amp and Amox also confirms their association on the formed AuNPs surface. Additionally, the intensity decrease for the C–S peak, this also reveals that sulphur atom in the thio-ether moiety is full incorporate in the antibiotic self-assembled monolayer on the gold nanoparticles surface.

Cytotoxicity of AuNPs and their intracellular localization inside viable cells

The toxicity of the 8 nm AuNPs and their cellular uptake inside the living cells is a key factor for evaluation their safety and also utility in biomedical and drug delivery applications (Guo et al. 2014). In this regard, the cytotoxicity of the AuNPs was evaluated in vitro against the cell lines in terms of their effect in various concentrations viz., 15.0, 30.0, 60.0, 125, 250 and 500 μg/ml on cell proliferation by the MTT assay. The results show that the dependent toxicity and the IC50 of AuNPs on HeLa cells is 48 μg/mL after 24 h of their exposure on HeLa cells. In reality, the metallic nanoparticles may fortify the reactive oxygen species (ROS) and effect in damage cellular components that ultimately lead to cell death (Vivek et al. 2012). On the other hand, the TEM analysis proves the successful entry of the Au NPs into the treated HeLa cells in comparison to the untreated cells (Fig. 5a). These nanoparticles were founded agglomerated inside the treated cells and localized inside the endosomes (Fig. 5b, c), revealing their internalization were through endocytosis, however further studies are needed to fully understand and elucidate their uptake mechanism inside the living cells.

Fig. 4 Characterization of the AuNPs and their conjugation with Amp, Amox. **a** X-ray diffraction pattern of Ampicillin (Amp), Amoxicillin (Amox), 8 nm diameter gold nanoparticles (AuNPs), Ampicillin loaded gold nanoparticles, Amoxicillin loaded gold nanoparticles, **b** FT-IR spectra of Ampicillin, Amoxicillin, gold nanoparticles, Ampicillin conjugated gold nanoparticles, and Amoxicillin conjugated gold nanoparticles) in the range of 1200–500 cm^{-1} **c** FT-IR in the range of 4000–1200 cm^{-1}

Effect of Au NPs on HeLa cells nucleic acid

The results show an induced cytotoxic effect by the Au NPs, including different apoptotic changes and nuclear condensation with fragmented/marginated chromatin structure as demonstrated by the AO/EtBr and DAPI staining methods. Furthermore, a complete nuclear damage with clear chromatin fragmentation was observed in the fluorescence images of the treated cells, without any evidence of nuclei breaking in the untreated Hela cells (Fig. 6). Based on the AO/EtBr stain observation, it is clear that the mechanism of cell death induced by AuNPs occurs via apoptosis. Where the orange color of the apoptotic/necrotic cells appears in red color in contrast with untreated controlled cells that appear healthy with green color (Fig. 6a, b). The results are in agreement with the nuclear degradation/fragmentation behavior in AuNPs treated cells that was reported by (Patra et al. 2007; Guo and Lu 2010; Khlifi et al. 2013; Alnasser et al. 2016). However, the confirmation of AuNPs penetration into cell membrane is still in progress. Those findings also were revealed by gel electrophoresis analysis, which showed clear intact DNA bands without any fragmentation or smearing with the untreated DNA (control), where there was no significant damage occurred. In contrast, the DNA of cells treated with IC50 concentration of AuNPs show the induction of apoptosis in interspersing smears in the lanes and substantial alter

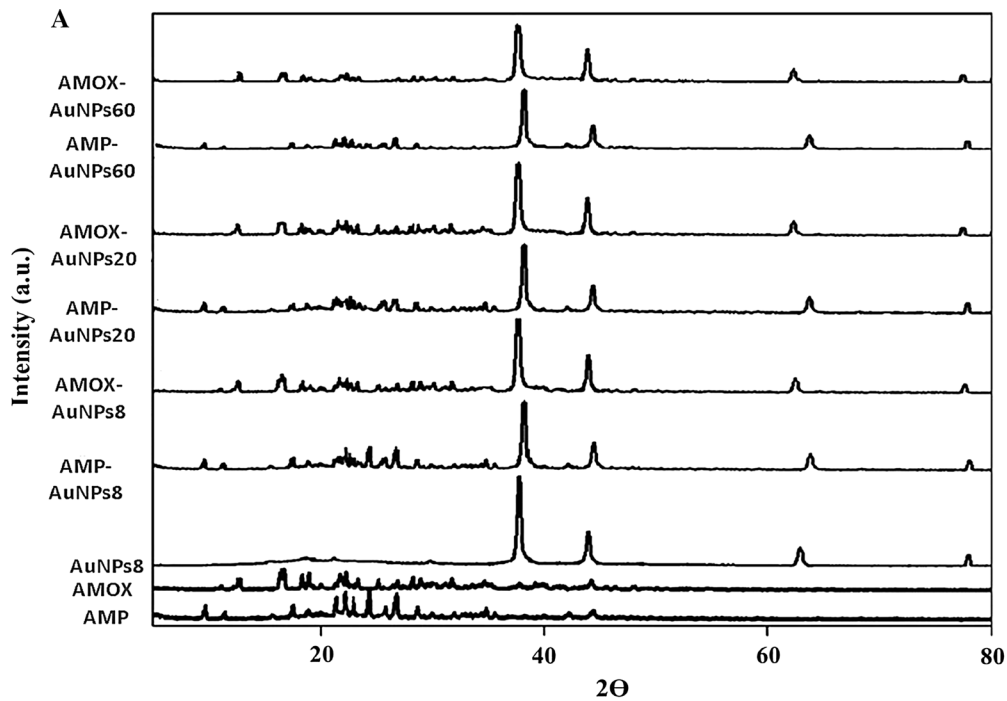
A
AMOX-AuNPs60
AMP-AuNPs60
AMOX-AuNPs20
AMP-AuNPs20
AMOX-AuNPs8
AMP-AuNPs8
AuNPs8
AMOX
AMP
Intensity (a.u.)
20
40
60
80
2Θ

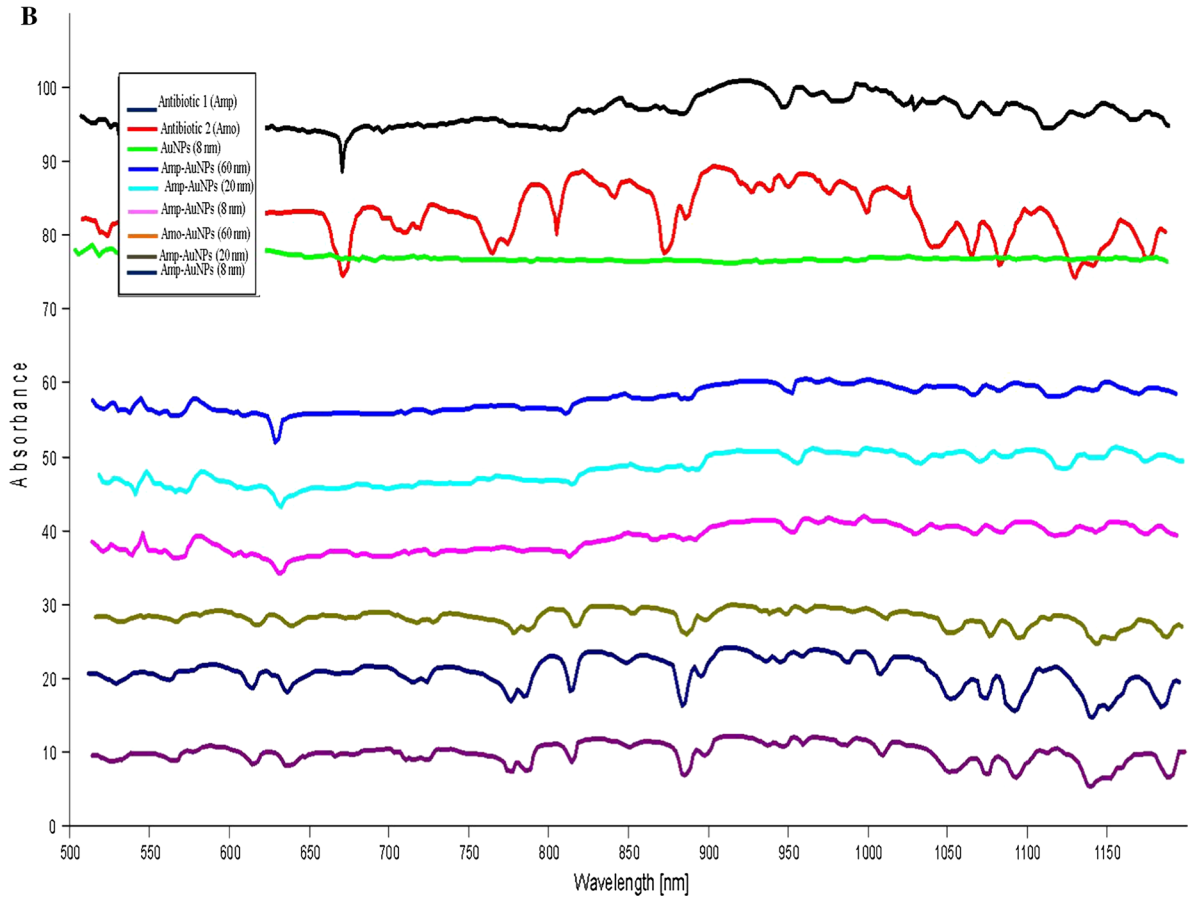
B
Antibiotic 1 (Amp)
Antibiotic 2 (Amo)
AuNPs (8 nm)
Amp-AuNPs (60 nm)
Amp-AuNPs (20 nm)
Amp-AuNPs (8 nm)
Amo-AuNPs (60 nm)
Amp-AuNPs (20 nm)
Amp-AuNPs (8 nm)
Absorbance
Wavelength [nm]

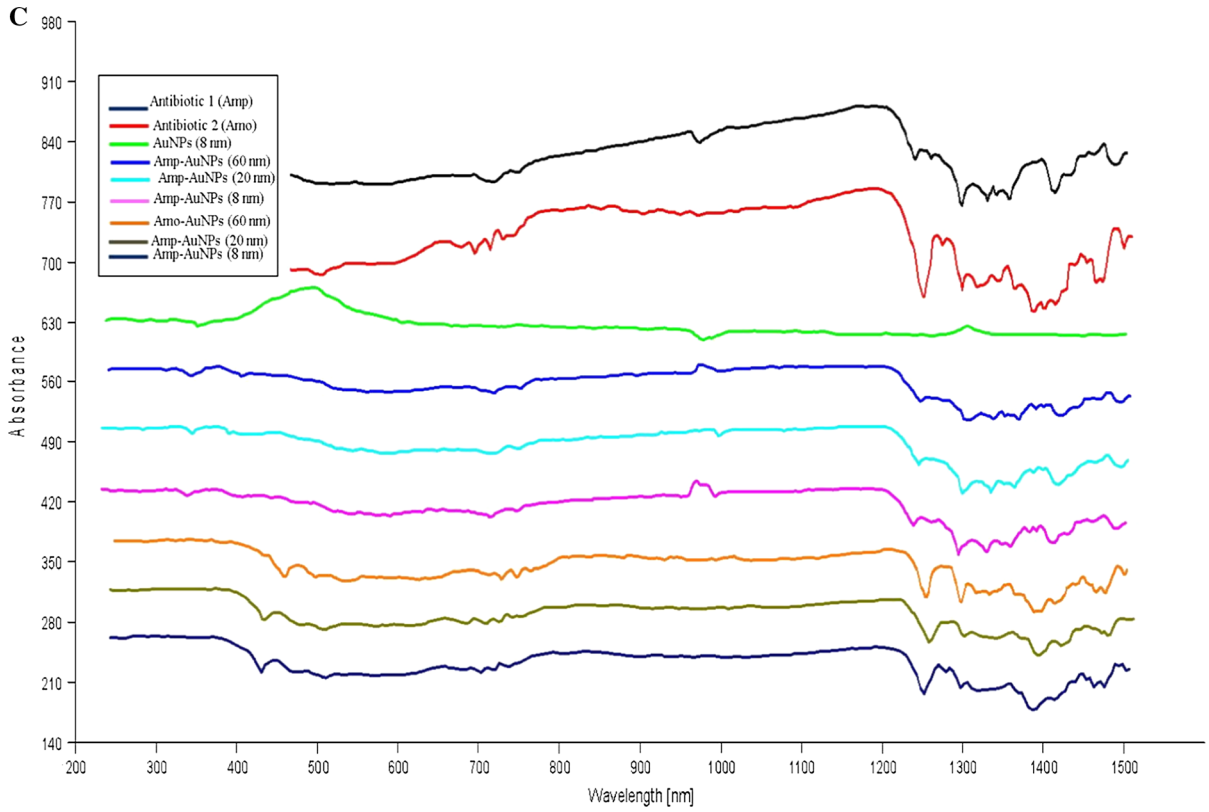

Fig. 4 continued

the electrophoretic migration within a time period of 24 h (Fig. 7). The smearing of DNA could occur due to some post-apoptotic HeLa cell necrosis. The results suggest that the decrement in the cell survival is caused by induction of DNA fragmentation and its direct chemical damage (Sriram et al. 2010). In this regard, the effect of Au NPs cytotoxicity on the HeLa cells is attributed to the potentiality of the mitochondrial dehydrogenase enzyme in the viable cells to cleave the tetrazolium rings of the pale yellow MTT and produce formazan crystals with blue color, which is hard to pass through the cell membranes (Konwarh et al. 2011). The NPs size and dose play a key role in toxicity due to the presence of protein/enzyme on their surfaces (Bellman 2015). While, the variability in cellular responses to the Au NPs may support the distinctive surface reactivity modulated by the presence of cytotoxic enzymes/proteins, contaminants, other poly-morphs and surface imperfections (Shi et al. 2015; Patil et al. 2018). The obtained results reveal the toxicity effect of Au NPs on cancer cells by inducing apoptosis in HeLa cells.

Ampicillin/Amoxicillin drug release (In-vitro)

Figure 8a, b shows the kinetics of drug release rate of Au NPs conjugated Ampicillin and Amoxicillin for different Au NPs sizes. The figure indicates a controlled release for ampicillin and Amoxicillin from the conjugated AuNPs surfaces. Interestingly, two biphasic release profiles are observed for both Ampicillin and Amoxicillin. The first short term and rapid release rate take about 6 h followed by a relatively slow steady and long term drug release, which is extended to a complete release for all the drug loaded on the AuNPs's surface. It is worth to mention that the drug release rate depends on the size of the Nanocarrier system exploited in the loading process (Table 1). Where, the smaller AuNPs (8 nm) the faster drug release rate (92%) after 24 h and archives

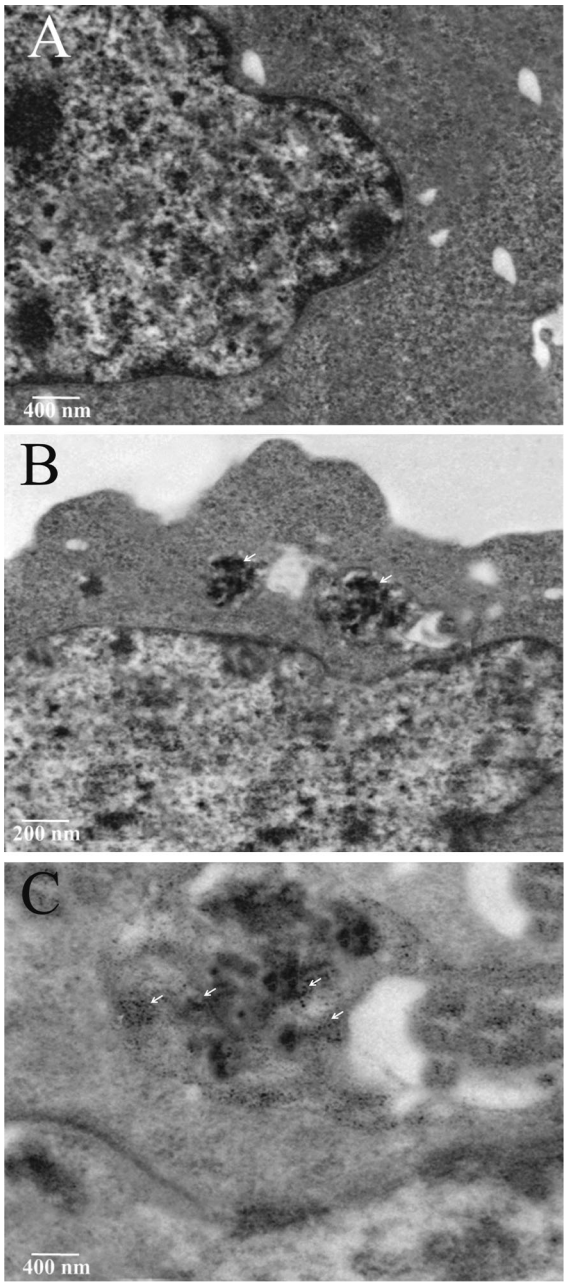

Fig. 5 Uptake and localization of AuNPs in HeLa cells: **a** control (untreated cells), **b** AuNPs-treated HeLa cells for 24 h showing AuNPs aggregates in the endosomes as black and electron dense spots (indicated by arrows). **c** Showing a cluster of individual nanoparticles inside treated cells

96% after 48 h, in contrast to the larger AuNPs of 60 nm that shows a release rate of 70%, 80% after 24 and 48 h, respectively. Similar results are also recorded for Amoxicillin. This significant behavior

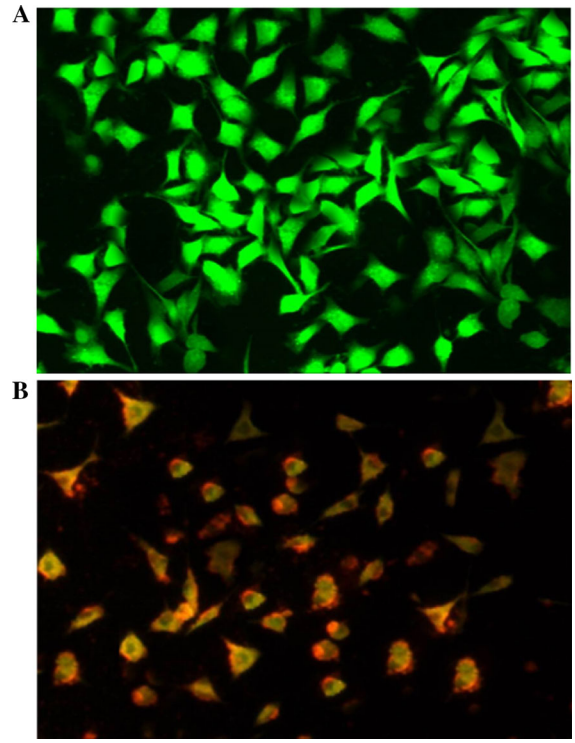

Fig. 6 Cytotoxic activity of the formed AuNPs: **a** fluorescence microscopic study of DAPI staining of control HeLa cells **b** gold nanoparticles treated HeLa cells

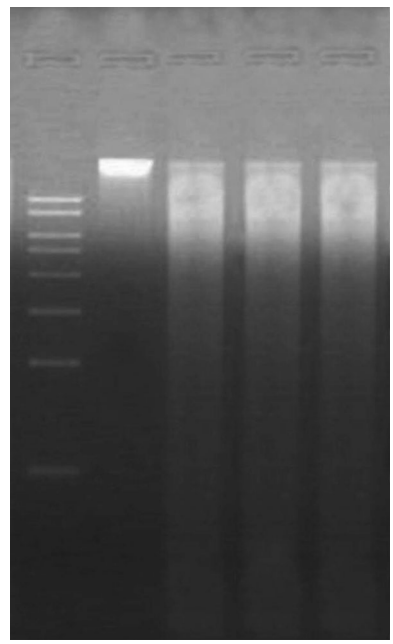

Fig. 7 DNA fragmentation of HeLa cells treated with biosynthesized AuNPs at 24 h: Lane 1: 1 kb DNA ladder, Lane 2: HeLa control DNA, Lane 3, 4 and 5: AuNPs treated (48 µg/mL)

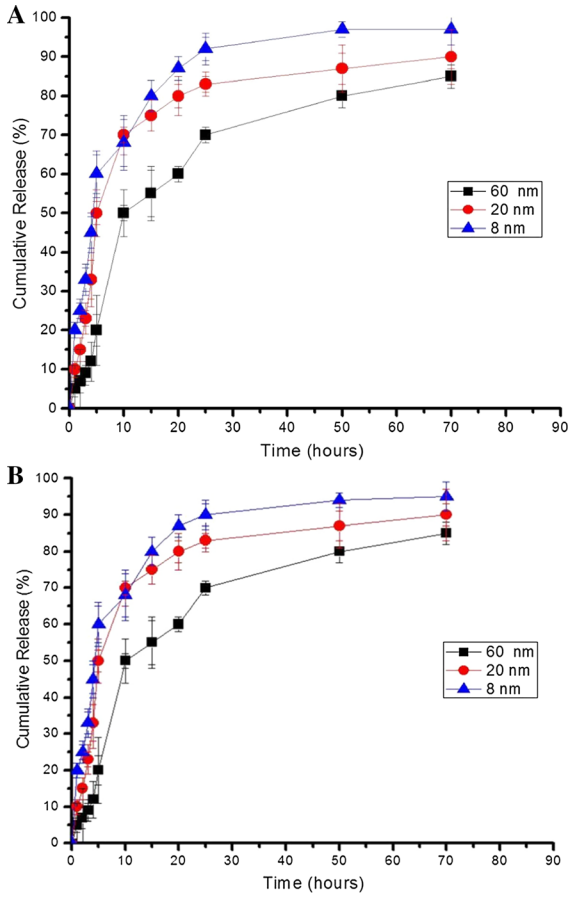

Fig. 8 Cumulative percentage of released Ampicillin: **a** and Amoxicillin (**b**), from the loaded gold nanoparticles of different particle sizes (8,20 and 60 nm) in PBS (pH 7.4) as a release media at 37 °C

is correlated to the larger surface area-to-volume ratio of the smaller AuNPs they obtained compared to the larger NPs. Thus, higher amount of the loaded drug with the same volume of NPs giving a higher probability of the drug molecules repulsion, leading to faster diffusion through the dialysis membrane. On the other hand, the AuNPs show a larger cores volume as the amount of the loading drug (Ampicillin/Amoxicillin) decreases, this means less repulsion force between the drug molecules and leads to slower release rate. Consequently, smaller tuned AuNPs size smaller, higher ampicillin/amoxicillin releasing rates.

On the other hand, the drug content for Ampicillin and Amoxicillin conjugated gold nano-particles was about 88.2 ± 4.8% and 82.4 ± 9.4%, respectively in case of the smallest AuNPs (8 nm). So, each milligram of Amp-AuNPs8 and Amox-AuNPs8 contains 0.88 and 0.82 mg of Ampicillin and Amoxicillin, respectively. The 20 nm nanoparticles showed 70.5 ± 6.2% and 72.8 ± 5.6%, loading for Ampicillin and amoxicillin, respectively. As well, the 60 nm nanoparticles showed a 74.2 ± 10.2% and 67.6 ± 7.5%, loading for Ampicillin and Amoxicillin, respectively. It should be mentioned that the measured Amp/Amox content in the supernatant was found to be the same to exclude the possibility of adsorption on the wall of the centrifuge tube. Meanwhile, the possibility of interfering of the supernatant of AuNPs with Ampicillin/Amoxicillin measurement was also excluded by the UV scanning of supernatant obtained after centrifugation of the prepared nanoparticles at 20,000 rpm for 30 min.

Antibacterial activity

Fifty-five Gram-negative bacterial isolates belong to *Pseudomonas aeruginosa*, *Enterobacter aerogenes*, and *Staphylococcus aureus* were assessed in vitro to study their susceptibility to Ampicillin (Amp) and Amoxicillin (Amox). The lowest susceptible bacterial

Table 1 Drug loading efficiency in relation to different sizes (8, 20, 60) nm of the biosynthesized gold nanoparticles (AuNPs)

Gold nanoparticles form	Loading efficiency (%)	Drug loading (%)
$AuNPs_8$ (alone)	–	–
$AuNPs_{40}$ (alone)	–	–
$AuNPs_{80}$ (alone)	–	–
Amp-$AuNPs_8$ (conjugated)	78 ± 2.1	88.2 ± 4.8
Amp-$AuNPs_{20}$ (conjugated)	59 ± 1.0	70.5 ± 6.2
Amp-$AuNPs_{60}$ (conjugated)	45 ± 2.7	74.2 ± 10.2
Amox-$AuNPs_8$ (conjugated)	71 ± 2.5	82.4 ± 9.4
Amox-$AuNPs_{20}$ (conjugated)	57 ± 1.5	72.8 ± 5.6
Amox-$AuNPs_{60}$ (conjugated)	47 ± 2.3	67.6 ± 7.5

isolates to Amp and Amox were selected to evaluate the antibacterial activity of Amp, Amox, and their conjugated formulations with the AuNPs (Amp-AuNPs and Amox-AuNPs). According to data presented in Table 2, the incubation of the unloaded Au NPs with either *Pseudomonas aeruginosa*, *Staphylococcus aureus* and *Enterobacter aerogenes* at 37 °C for 24 h did not show any suppression in the pathogenic bacterial growth. While, the bacterial growth suppression is observed with both free Ampicillin, Amoxicillin and with conjugated Au NPs. Interestingly, the results clearly prove that both conjugated Au NPs show higher antibacterial activity in comparison with the pure Au NPs. The antibacterial activity of conjugated Amp AuNPs are in the order of Amp -AuNPs8 > Amp -AuNPs20 > Amp -AuNPs60 > Amp. Similarly, for Amox, it is in the order of Mem-AuNPs8 > Amox -AuNPs20 = Amox -AuNPs60 > Amox. Meaning, that as the Amp/Amox formulated AuNPs size decrease as their antibacterial activity increase. This is also supported by the 3–4 folds decrease in the MIC value for the Amp -AuNPs versus *P. aeruginosa*, respectively. While, the Amp -AuNPs20 and Amp -AuNPs60 reduce the MICs values only by 2-fold, respectively. On the same way, Amox loaded AuNPs8 significantly decreases the MICs of the Amox versus *S. aureus* and *E. aerogenes* by more than 2–3 folds, respectively. Hence, it can be concluded that the Amp-AuNPs8 and Amox -AuNPs8 versus Gram negative Antibiotic-resistant isolates introduce a superior activity in comparison with to the free antibiotics (Table 2). formulation as AuNPs8 reduced the MICs below the CLSI breakpoint for Amp and Amox according to CLSI guidelines, 2015. In this regards, the data prove that the antibacterial action can be introduced by loading these drugs on the AuNPs surface, therefore it shows high restore potentiality for their actions against bacteria and using also a small size nanomaterials to gain a successful and better results. Furthermore, the killing rate of both Amp/Amox loaded AuNPs against Antibiotic resistant bacteria was also evaluated for *S. aureus* and *P. aeruginosa* isolates after their incubation with Amp-AuNPs8 and Amox-AuNPs8 and count the lining bacteria at different time intervals. The results indicate that the Amp-AuNPs8 formulation is able to kill the *S. aureus* rapidly. The bacterial count data reveals that after 1 h of incubation with Ipm-AuNPs8, the *S. aureus* shows a drastic drop in the living bacterial cells from 1.6×10^6 colony forming unit (CFU)/ml to 1.6×10^4 CFU/ml with complete bacterial death after 24 h (Fig. 9a). Similarly, Mem-AuNPs8 rapidly killed Ks1.0 (Fig. 9b) after only 2 h of incubation and completely killed all viable bacteria after only 5 h of incubation. We can conclude that the formulation of conjugated Au NPs enhances the antibacterial action of the two studied antibiotics against antibiotic resistant bacteria. The antibacterial action of the amoxicillin conjugated AuNPs is greater than the ampicillin conjugated AuNPs (Table 2), (Amp: Ampicillin; Amox: Amoxicillin; AuNPs8, AuNPs20 and AuNPs60: are gold nanoparticles size 8, 20 and 60 nm

Table 2 The minimum inhibitory concentration (MIC) of Ampicillin and Amoxicillin compared to their conjugated gold nanoparticles in different sizes against different infectious G -Ve bacteria (n = 3)

	The minimal inhibitory concentration (MIC-μg/ml)					
	Pseudomonas aeruginosa		*Staphylococcus aureus*		*Enterobacter aerogenes*	
	St.1.0	St.2.0	St.1.0	St.2.0	St.1.0	St2.0
Amp	27	29	35	42	49	52
Amp-AuNPs$_8$	1	1.5	3	4.5	3	2
Amp-AuNPs$_{20}$	4	4	8	10	5	7
Amp-AuNPs$_{60}$	7	6.5	12	14	11	14
Amox	12	14	26	22	27	24
Amox-AuNPs$_8$	0.5	0.5	2.5	2	4	3
Amox-AuNPs$_{20}$	1.5	1.5	5	3	8	7
Amox-AuNPs$_{60}$	2	4	8	6	12	15
AuNPs$_8$	NE		NE		NE	
AuNPs$_{20}$	NE		NE		NE	
AuNPs$_{60}$	NE		NE		NE	

Amp Ampicillin; *Amox* Amoxicillin; *AuNPs$_8$, AuNPs$_{20}$ and AuNPs$_{60}$* are gold nanoparticles size 8, 20 and 60 nm respectively and *NE* no antibacterial effect

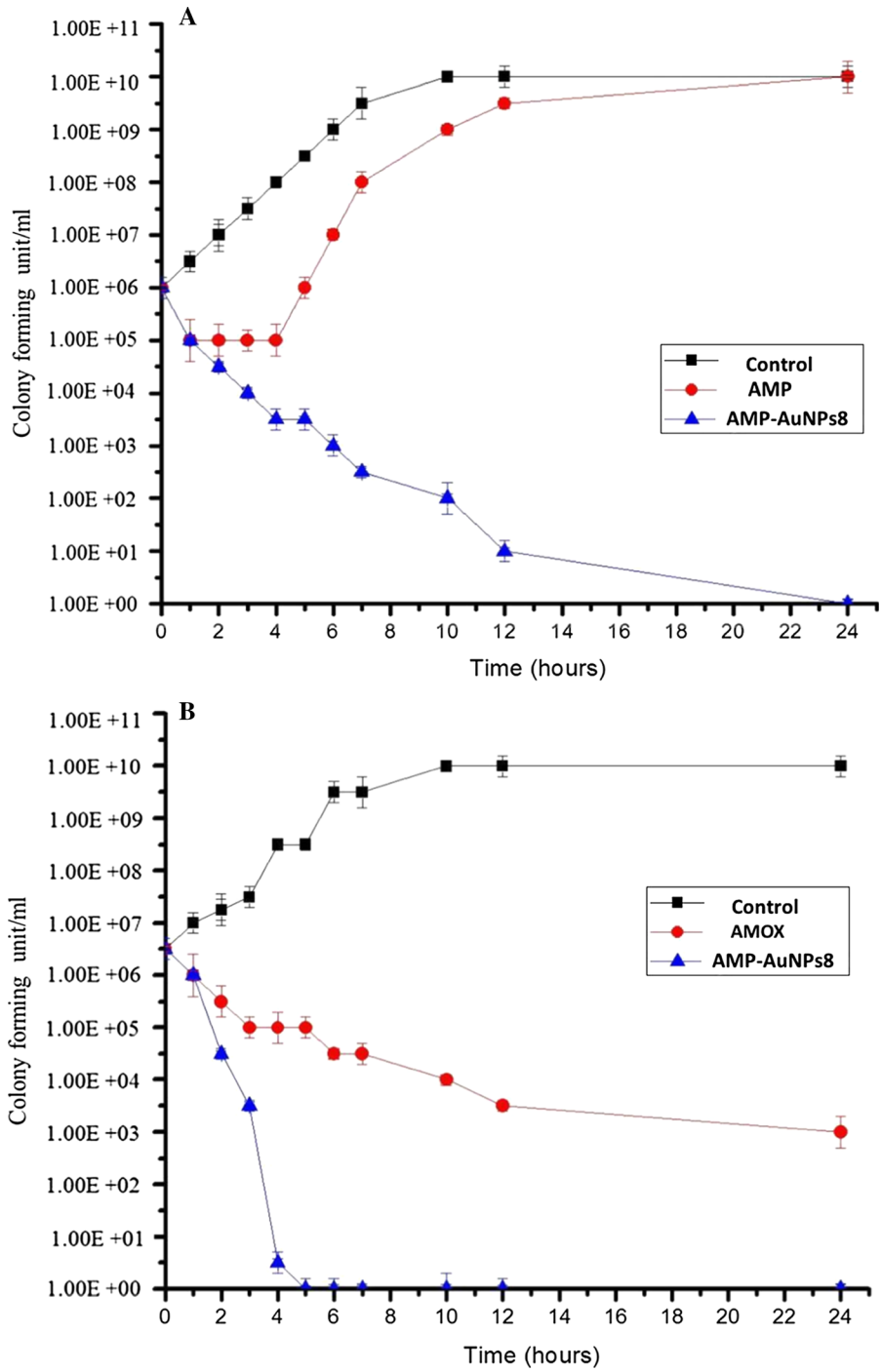

Fig. 9 Time kill assay of *Staphylococcus aureus* treated with: **a** free Ampicillin (Amp) and 8 nm diameter Ampicillin loaded gold nanoparticles (Amp-AuNPs8); **b** free Amoxicillin (Amox) and 8 nm diameter Amoxicillin loaded gold nanoparticles (Mem-AuNPs8), compared to control antibiotic free culture

respectively and NE: no antibacterial effect). This refers to the superiority of the amoxicillin molecules over ampicillin ones in suppressing the bacterial cell wall synthesis (Nicolau 2008). Different reports reveale that amoxicillin has more affinity to PBPs compared to the ampicillin (Bax et al. 1989; Kuo et al. 2016). The amoxicillin molecules show more functionality more than the ampicillin molecules, where it interacts strongly and diffuses through the outer bacteria membrane, which refers to its better reactivity

against Gram -Ve bacilli in comparison with the amoxicillin. However, the Amp-AuNPs and Amox-AuNPs are valuable antibacterial agents due to their great killing effect of different multi-resistance bacteria. The decrease in the Au NPs size increases the adsorption area to carry more antibiotics on the surface and improves the suppression rate in bacterial growth. The results are in agreements with (Brown et al. 2012; Rastogi et al. 2012; Kuo et al. 2016; Payne et al. 2016). It worth to mention that only few works that investigate the antimicrobial effect of AuNPs against microbial pathogens (Zhou et al. 2012; Lima et al. 2013), which increases/synergizes the action of these conjugated NPs, as a result of the direct interaction between the free antibiotics and the loaded AuNPs from one side and the bacterial cells from the other one (Kuo et al. 2016). However, in the presented work all the Au NPs don't show any bactericidal effect on all the tested bacterial growth (Tables 2), whereas antibiotics retained their antibacterial action proficiency upon conjugation on the surface of the AuNPs. However, the mechanistic antibacterial effect of the conjugated AuNPs is less understood till now. The observed improve in the antimicrobial activity of a drug conjugated AuNPs refers to two different reasons (Gupta et al. 2016). The first reason refers to the large AuNPs surface area that permits a better chance for loading large amount of antibiotics that have the potential to interact and bind to the PBP receptor site as a single molecule, leading to better attachment of the antibiotic molecules on the outer bacterial cell membrane in comparison with the free antibiotic (Gu et al. 2003; Gupta et al. 2016). As a result, the accumulation of antibiotic with this high concentration it allows to disturb the osmotic bacterial membrane balance and also inhibit or reduce the cell wall synthesis of the bacterial cell pathogen (Grace and Pandian 2007). The second reason is the high possibility offered to the loaded drug to target multiple sites on the bacteria cell surface and penetrate their cell wall. Consequently block the sulphur containing proteins as well as the phosphorous in the nucleic acid (i.e. DNA) (Cui et al. 2012; Khan et al. 2013; Kandimalla et al. 2016). In spite of these findings, more comprehensive biocompatible studies are needed as a prerequisite to qualify the formulated gold nano-carriers as a clinically accepted delivery transporter before considering this protocol for clinical application (Khan et al. 2013). This may be due to the lack of complete understanding of these unique nanomaterials regarding their toxicity, accumulation and elimination inside the human body. In the past few years, several reports showed a great bio-distribution after IV administration in the different organs/tissues of liver (Balasubramanian et al. 2010; Morais et al. 2012), however few reports indicated the sequential hepato-biliary track for their execration (Zhang et al. 2016). In conclusion, a better understanding of biocompatibility of those smart pharmaceutical nano-carriers (showing interesting anticancer and antibacterial activity) is really required to reinforce their implementations in clinical therapy.

Conclusions

In the present work, we report a one step, safe and rapid method (5 min) for the AuNPs synthesis using aqueous extract of the freshwater fungus *J. aquatica* that is developed for the first time. To the best of our knowledge, freshwater fungi are never exploited in nanomaterials synthesis. The potentiality of different sizes of the produced AuNPs to working as antibiotic delivery system was evaluated for the therapy of multi-resistant human pathogenic bacteria. The results indicated the successful conjugation of both ampicillin and amoxicillin antibiotics with the gold nanoparticles surface, suggesting the presence of a promising chance with unique antibacterial effect for antibiotic -loaded AuNPs over free drug. The potential efficiency of the AuNPs loading is improved with the smaller AuNPs size than the larger sizes. Moreover, the produced AuNPs showed a dose-dependent cytotoxicity against Hela cancer cells provided with appearance of apoptosis observation, suggesting their possible use as a reliable tumor-targeted drug carrier system. A possible mode of effective cytotoxic action of the mycosynthesized AuNPs has been clarified through molecular studies. However, more studies are required in vivo clinical application for authenticating the application of the above mentioned material. Undoubtedly, this simple procedure for the biosynthesis of AuNPs with its unique merits has several advantages including cost effectiveness, simplicity, possibility for cancer treatment as well as improvement and delivering either antibiotic or any other drug in biomedical and pharmaceutical applications with large-scale commercial production. Most importantly, the commercial

production of a dry powdered functionalized antibiotic conjugated AuNPs formula to be used as new intravenous infusion is a promising study that will be the core of interest in the future.

Acknowledgements Mohamed A. Mohamed is acknowledge the extended support by Prof. Jose Anotino Daròs, and all his laboratory facilities supported by Grant BIO2014-54,269-R from the Spanish Ministerio Economía y Competividad (MINECO, Spain). The author is also greatly thankful to the Electron Microscopy Service Unit and the Valencia Nanophotonics Technology Center at Universitat Politècnica de València for their technical support.

Author contributions MAM designed the study. He wrote, revised and approved the final version of the manuscript before submission.

Compliance with ethical standards

Conflicts of interest The authors declare no conflict of interest and no competing financial interests.

Research involving human and animal participants This article does not contain any studies with human participants or animals performed by any of the authors.

References

Abdel-Hafez SI, Nafady NA, Abdel-Rahim IR, Shaltout AM, Daròs JA, Mohamed MA (2016) Assessment of protein silver nanoparticles toxicity against pathogenic *Alternaria solani*. 3 Biotech 6(2):199

Alnasser Y, Ferradas C, Clark T, Calderon M, Gurbillon A, Gamboa D, Vinetz JM (2016) Colorimetric detection of *Plasmodium vivax* in urine using MSP10 oligonucleotides and gold nanoparticles. PLoS Negl Trop Des 10(10):e0005029

Baghizadeh A, Ranjbar S, Gupta VK, Asif M, Pourseyedi S, Karimi MJ, Mohammadinejad R (2015) Green synthesis of silver nanoparticles using seed extract of *Calendula officinalis* in liquid phase. J Mol Liq 207:159–163

Balasooriya ER, Jayasinghe CD, Jayawardena UA, Ruwanthika RWD, Mendis de Silva R, Udagama PV (2017) Honey mediated green synthesis of nanoparticles: new era of safe nanotechnology. J Nanomater. https://doi.org/10.1155/2017/5919836

Balasubramanian SK, Jittiwat J, Manikandan J, Ong CN, Liya EY, Ong WY (2010) Biodistribution of gold nanoparticles and gene expression changes in the liver and spleen after intravenous administration in rats. Biomaterials 31(8):2034–2042

Barbosa HR, Rodrigues MFA, Campos CC, Chaves ME, Nunes I, Juliano Y, Novo NF (1995) Counting of viable cluster-forming and non cluster-forming bacteria: a comparison between the drop and the spread methods. J Microbiol Methods 22(1):39–50

Baroud Á, Dandache I, Araj GF, Wakim R, Kanj S, Kanafani Z, Matar GM (2013) Underlying mechanisms of carbapenem resistance in extended-spectrum β-lactamase-producing *Klebsiella pneumoniae* and *Escherichia coli* isolates at a tertiary care centre in Lebanon: role of OXA-48 and NDM-1 carbapenemases. Int J Antimicrob Agents 41(1):75–79

Bax RP, Bastain W, Featherstone A, Wilkinson DM, Hutchison M (1989) The pharmacokinetics of meropenem in volunteers. J Antimicrob Chemother 24(suppl_A):311–320

Bellman RE (2015) Adaptive control processes: a guided tour, vol 2045. Princeton University Press, Princeton

Boone DR, Castenholz RW, Garrity GM (2001) Bergey's manual of systematic bacteriology. Springer, New York

Brown AN, Smith K, Samuels TA, Lu J, Obare SO, Scott ME (2012) Nanoparticles functionalized with ampicillin destroy multiple-antibiotic-resistant isolates of *Pseudomonas aeruginosa* and *Enterobacter aerogenes* and methicillin-resistant *Staphylococcus aureus*. Appl Environ Microbiol 78(8):2768–2774

Chen YL, Li QZ (2007) Prediction of apoptosis protein subcellular location using improved hybrid approach and pseudo-amino acid composition. J Theor Biol 248(2):377–381

Choi HH (1999) On the existence of linear sliding surfaces for a class of uncertain dynamic systems with mismatched uncertainties. Automatica 35(10):1707–1715

Cui Y, Zhao Y, Tian Y, Zhang W, Lü X, Jiang X (2012) The molecular mechanism of action of bactericidal gold nanoparticles on *Escherichia coli*. Biomaterials 33(7):2327–2333

Delcaru C, Podgoreanu P, Alexandru I, Popescu N, Măruţescu L, Bleotu C, Lazăr V (2017) Antibiotic resistance and virulence phenotypes of recent bacterial strains isolated from urinary tract infections in elderly patients with prostatic disease. J Pathog 6(2):22

Dhamecha D, Jalalpure S, Jadhav K, Jagwani S, Chavan R (2016) Doxorubicin loaded gold nanoparticles: implication of passive targeting on anticancer efficacy. Pharmacol Res 113:547–556

Dhar S, Reddy EM, Shiras A, Pokharkar V, Prasad BEE (2008) Natural gum reduced/stabilized gold nanoparticles for drug delivery formulations. Chem Eur J 14(33):10244–10250

Foo Y, Periasamy V, Kiew L, Kumar G, Malek S (2017) Curcuma mangga-mediated synthesis of gold nanoparticles: characterization, stability, cytotoxicity, and blood compatibility. Nanomaterials 7(6):123

Gannimani R, Ramesh M, Mtambo S, Pillay K, Soliman ME, Govender P (2016) γ-Cyclodextrin capped silver nanoparticles for molecular recognition and enhancement of antibacterial activity of chloramphenicol. J Inorg Biochem 157:15–24

Goh TK, Hyde KD (1999) Fungi on submerged wood and bamboo in the Plover Cove Reservoir, Hong Kong. Fungal Diversity 3:57–85

Grace AN, Pandian K (2007) Quinolone antibiotic-capped gold nanoparticles and their antibacterial efficacy against gram positive and gram negative organisms. J Bionanosci 1(2):96–105

Gu H, Ho PL, Tong E, Wang L, Xu B (2003) Presenting vancomycin on nanoparticles to enhance antimicrobial activities. Nano Lett 3(9):1261–1263

Guo L, Lu Z (2010) The fate of miRNA* strand through evolutionary analysis: implication for degradation as merely carrier strand or potential regulatory molecule? PLoS ONE 5(6):e11387

Guo D, Zhao Y, Zhang Y, Wang Q, Huang Z, Ding Q, Gu N (2014) The cellular uptake and cytotoxic effect of silver nanoparticles on chronic myeloid leukemia cells. J Biomed Nanotech 10(4):669–678

Gupta A, Landis RF, Rotello VM (2016) Nanoparticle-based antimicrobials: surface functionality is critical. F1000Research. https://doi.org/10.12688/f1000research.7595.1

Harsha S (2012) Dual drug delivery system for targeting *H. pylori* in the stomach: preparation and in vitro characterization of amoxicillin-loaded Carbopol® nanospheres. Int J Nanomedicine 7:4787

Hernández-Carlos B, Gamboa-Angulo MM (2011) Metabolites from freshwater aquatic microalgae and fungi as potential natural pesticides. Phytochem Rev 10(2):261–286

Kandimalla R, Kalita S, Saikia B, Choudhury B, Singh YP, Kalita K, Kotoky J (2016) Antioxidant and hepatoprotective potentiality of Randia dumetorum Lam. Leaf and bark via inhibition of oxidative stress and inflammatory cytokines. Front Pharmacol 7:205

Kasthuri J, Veerapandian S, Rajendiran N (2009) Biological synthesis of silver and gold nanoparticles using apiin as reducing agent. Colloids Surf B 68(1):55–60

Khan MS, Vishakante GD, Siddaramaiah H (2013) Gold nanoparticles: a paradigm shift in biomedical applications. Adv Colloid Interfac 199:44–58

Khlifi D, Hayouni EA, Valentin A, Cazaux S, Moukarzel B, Hamdi M, Bouajila J (2013) LC–MS analysis, anticancer, antioxidant and antimalarial activities of *Cynodon dactylon* L. extracts. Ind Crop Prod 45:240–247

Kim DY, Kim M, Shinde S, Sung JS, Ghodake G (2017) Cytotoxicity and antibacterial assessment of gallic acid capped gold nanoparticles. Colloids Surf B 149:162–167

Konwarh R, Gogoi B, Philip R, Laskar MA, Karak N (2011) Biomimetic preparation of polymer-supported free radical scavenging, cytocompatible and antimicrobial "green" silver nanoparticles using aqueous extract of *Citrus sinensis* peel. Colloids Surf B 84(2):338–345

Kuo YL, Wang SG, Wu CY, Lee KC, Jao CJ, Chou SH, Chen YC (2016) Functional gold nanoparticle-based antibacterial agents for nosocomial and antibiotic-resistant bacteria. Nanomedicine 11(19):2497–2510

Lien L, Lan P, Chuc N, Hoa N, Nhung P, Thoa N, Stålsby Lundborg C (2017) Antibiotic resistance and antibiotic resistance genes in *Escherichia coli* isolates from hospital wastewater in Vietnam. Int J Environ Res Public Health 14(7):699

Lima E, Guerra R, Lara V, Guzmán A (2013) Gold nanoparticles as efficient antimicrobial agents for *Escherichia coli* and *Salmonella typhi*. Chem Cent J 7(1):11

Maity P, Bepari M, Pradhan A, Baral R, Roy S, Choudhury SM (2018) Synthesis and characterization of biogenic metal nanoparticles and its cytotoxicity and anti-neoplasticity through the induction of oxidative stress, mitochondrial dysfunction and apoptosis. Colloids Surf B 161:111–120

Miliani K, L'Hériteau F, Lacave L, Carbonne A, Astagneau P, Antimicrobial Surveillance Network Study Group (2011) Imipenem and ciprofloxacin consumption as factors associated with high incidence rates of resistant *Pseudomonas aeruginosa* in hospitals in northern France. J Hosp Infect 77(4):343–347

Morais T, Soares ME, Duarte JA, Soares L, Maia S, Gomes P, de Lourdes Bastos M (2012) Effect of surface coating on the biodistribution profile of gold nanoparticles in the rat. Eur J Pharm Biopharm 80(1):185–193

Mori T, Hegmann T (2016) Determining the composition of gold nanoparticles: a compilation of shapes, sizes, and calculations using geometric considerations. J Nanopart 18(10):295

Nicolau DP (2008) Carbapenems: a potent class of antibiotics. Expert Opin Pharmacother 9(1):23–37

Onuigbo E, Onugwu A, Nwocha M, Odiase A, Attama A (2016) Preparation and in vitro evaluation of amoxicillin encapsulated in alginate-coated chitosan microparticles. Trop J Pharm Res 15(11):2303–2309

Paczkowska M, Mizera M, Szymanowska-Powałowska D, Lewandowska K, Błaszczak W, Gościańska J, Cielecka-Piontek J (2016) β-Cyclodextrin complexation as an effective drug delivery system for meropenem. Eur J Pharm Biopharm 99:24–34

Patil MP, Ngabire D, Thi HHP, Kim MD, Kim GD (2017) Eco-friendly synthesis of gold nanoparticles and evaluation of their cytotoxic activity on cancer cells. J Cluster Sci 28(1):119–132

Patil MP, Jin X, Simeon NC, Palma J, Kim D, Ngabire D, Kim GD (2018) Anticancer activity of Sasa borealis leaf extract-mediated gold nanoparticles. Artif Cell Nanomed B 46(1):82–88

Patra HK, Banerjee S, Chaudhuri U, Lahiri P, Dasgupta AK (2007) Cell selective response to gold nanoparticles. Nanomedicine 3(2):111–119

Payne JN, Waghwani HK, Connor MG, Hamilton W, Tockstein S, Moolani H, Dakshinamurthy R (2016) Novel synthesis of kanamycin conjugated gold nanoparticles with potent antibacterial activity. Front Microbiol 7:607

Poojary MM, Passamonti P, Adhikari AV (2016) Green synthesis of silver and gold nanoparticles using root bark extract of *Mammea suriga*: characterization, process optimization, and their antibacterial activity. BioNanoScience 6(2):110–120

Rastogi L, Kora AJ, Arunachalam J (2012) Highly stable, protein capped gold nanoparticles as effective drug delivery vehicles for amino-glycosidic antibiotics. Mater Sci Eng R C 32(6):1571–1577

Rohman A, Silawati D, Riyanto S (2015) Simultaneous determination of sulfamethoxazole and trimethoprim using UV spectroscopy in combination with multivariate calibration. Int J Med Sci 15(4):178

Roy P, Saha SK, Gayen P, Chowdhury P, Sinha Babu SP (2018) Exploration of antifilarial activity of gold nanoparticle against human and bovine filarial parasites: a nanomedicinal mechanistic approach. Colloids Surf B 161:236–243. https://doi.org/10.1016/j.colsurfb.2017.10.057

Shameli K, Bin Ahmad M, Jazayeri SD, Sedaghat S, Shabanzadeh P, Jahangirian H, Abdollahi Y (2012) Synthesis and characterization of polyethylene glycol mediated silver nanoparticles by the green method. Int J Mol Sci 13(6):6639–6650

Shi C, Zhu N, Cao Y, Wu P (2015) Biosynthesis of gold nanoparticles assisted by the intracellular protein extract of *Pycnoporus sanguineus* and its catalysis in degradation of 4-nitroaniline. Nanoscale Res Lett 10(1):147

Sotgiu G, D'Ambrosio L, Centis R, Tiberi S, Esposito S, Dore S, Migliori G (2016) Carbapenems to treat multidrug and extensively drug-resistant tuberculosis: a systematic review. Int J Mol Sci 17(3):373

Sriram MI, Kanth SBM, Kalishwaralal K, Gurunathan S (2010) Antitumor activity of silver nanoparticles in Dalton's lymphoma ascites tumor model. Int J Nanomedicine 5:753

Sun Y, Wang L, Li J, Zhao C, Zhao J, Liu M, Wen A (2014) Synergistic efficacy of meropenem and rifampicin in a murine model of sepsis caused by multidrug-resistant *Acinetobacter baumannii*. Eur J Pharmacol 729:116–122

Tang HJ, Hsieh CF, Chang PC, Chen JJ, Lin YH, Lai CC, Chuang YC (2016) Clinical significance of community-and healthcare-acquired carbapenem-resistant Enterobacteriaceae isolates. PLoS ONE 11(3):e0151897

Thomas R, Nair AP, Soumya KR, Mathew J, Radhakrishnan EK (2014) Antibacterial activity and synergistic effect of biosynthesized AgNPs with antibiotics against multidrug-resistant biofilm-forming coagulase-negative staphylococci isolated from clinical samples. Biotechnol Appl Biochem 173(2):449–460

Vivek R, Thangam R, Muthuchelian K, Gunasekaran P, Kaveri K, Kannan S (2012) Green biosynthesis of silver nanoparticles from *Annona squamosa* leaf extract and its in vitro cytotoxic effect on MCF-7 cells. Process Biochem 47(12):2405–2410

Yang H, Lv N, Hu L, Liu Y, Cheng J, Ye Y, Li J (2016) In vivo activity of vancomycin combined with colistin against multidrug-resistant strains of *Acinetobacter baumannii* in a *Galleria mellonella* model. J Infect Dis 48(3):189–194

Yuan W, Kuai R, Dai Z, Yuan Y, Zheng N, Jiang W, Schwendeman A (2017a) Development of a flow-through USP-4 apparatus drug release assay to evaluate doxorubicin liposomes. AAPS J 19(1):150–160

Yuan CG, Huo C, Yu S, Gui B (2017b) Biosynthesis of gold nanoparticles using *Capsicum annuum* var. grossum pulp extract and its catalytic activity. Physica E 85:19–26

Zhang YN, Poon W, Tavares AJ, McGilvray ID, Chan WC (2016) Nanoparticle–liver interactions: cellular uptake and hepatobiliary elimination. J Control Release 240:332–348

Zhou Y, Kong Y, Kundu S, Cirillo JD, Liang H (2012) Antibacterial activities of gold and silver nanoparticles against *Escherichia coli* and bacillus Calmette-Guérin. J Nanobiotechnol 10(1):19